



Optimization of an Occulter-Based Extrasolar-Planet-Imaging Mission

Egemen Kolemen*

Princeton Plasma Physics Laboratory, Princeton, New Jersey 08543

and

N. Jeremy Kasdin†

Princeton University, Princeton, New Jersey 08544

DOI: 10.2514/1.53479

A novel approach to extrasolar-planet imaging uses a pair of satellites: a telescope and an occulter, where the latter is placed in the line of sight between the telescope and the star system to be imaged in order to enhance the telescope's imaging capability. The optimal configuration of this satellite formation around sun–Earth L2 halo orbits is studied. Trajectory optimization of the occulter motion between imaging sessions of different stars is performed using a range of different criteria and methods. Thus, the global optimization problem is transformed into a time-dependent traveling salesman problem. The time-dependent traveling salesman problem is augmented with various constraints that arrive from the mission, and this problem is solved by employing simulated annealing and branching algorithms. For a concrete understanding of the feasibility of the mission, the performance of an example spacecraft, the Small Missions for Advanced Research in Technology (SMART-1), is analyzed.

I. Introduction

IT IS likely that the next decade will see NASA launch the first mission to detect, image, and characterize extrasolar Earth-like planets. Current work is directed at studying a variety of architecture concepts and the associated optical engineering in order to prove the feasibility of a mission. The challenges in such a mission are many; chief among them is creating the necessary high contrast to image an Earth-like planet despite its small angular separation and its 10^{-10} intensity ratio relative to the host star. Many approaches have been proposed to achieve the needed contrast employing either separated satellite interferometers, coronagraphs internal to a large telescope, or external occulters, where a large screen is flown far from the telescope to block the incoming starlight (see, e.g., Beckwith [1] for a summary). While all have much the same scientific potential, they differ greatly in their technological challenges. While internal coronagraphs only need a single filled aperture telescope, they require complex wavefront control systems to compensate for the inevitable optical distortions. External occulters are appealing because they remove the starlight from the telescope completely, eliminating the need for wavefront control. However, they add the challenge of precisely manufacturing the occulter and flying it in formation with the telescope. In this paper, an occulter-based mission scenario and study optimal approaches to an observing program are examined.

An occulter is a large, opaque screen, tens of meters in diameter, flown 50,000 km or more from a conventional telescope, anywhere from 2 to 4 m in diameter or larger; the arrangement is schematically shown in Fig. 1. Such a concept for planet finding was first proposed by Spitzer [2] using an apodized screen and later again by Marchal [3] employing shaped projections around the edges. Since then, a number of proposals have been put forward employing apodized screens (Copi and Starkman [4] and Schultz et al. [5]) or, more recently, shaped occulters as shown in Fig. 1 (Simmons [6], Cash et al. [7], and Kasdin et al. [8]). Vanderbei et al. [9] describe how the

shape of the occulter can be optimized to achieve the needed suppression at the smallest possible size and separation from the telescope.

Most mission concepts consist of flying a large telescope in a halo orbit about the sun–Earth L2 point (for details about the dynamics around L2, see Kolemen et al. [10]) with the large occulter flying in formation along the line of sight (LOS) to each target star, as shown in Fig. 2 (see Cash et al. [11]). In this paper, the alignment control problem is not discussed. Rather, approaches for determining the transfer trajectory of the occulter from one target star to another and for building a complete mission scenario for a particular population of targets is studied. The objective is to enable the imaging of the largest possible number of planetary systems while minimizing the total mass of the occulter spacecraft (dry mass and fuel). As more control is used, scientific achievement (that is, the number of planetary systems that are imaged) is higher but so is the cost due to thruster weight and fuel consumption. The results described in this paper enable a trade study, incorporating different thrusters and imaging different star systems, in terms of cost and scientific achievement.

The control problem can be separated into two parts: the LOS control of the formation during imaging and the trajectory control for realignment between imaging sessions. Since fuel use is dominated by the realignment, the study was focused there to find estimates of the total fuel consumption. First, the optimal control problem for a given realignment is solved. This provides the optimal trajectories that take the occulter from a given star LOS to another LOS. Employing Euler–Lagrange, sequential quadratic programming (SQP) and shooting algorithms, the energy, time, and fuel-optimal control for continuous thrusters were obtained. The results of each method are then compared.

After finding the relevant minimum-fuel trajectories between all pairs of target stars, the sequencing and timing of the imaging session is examined in order to minimize global fuel consumption. To keep the analysis tractable, the time spent during an imaging session is ignored, and thus the natural dynamics that occurs. The error doing so is small since the realignment time is expected to be so much longer than the imaging time. While it may be possible to use the natural dynamics during an imaging session to find slightly lower cost trajectories for realignment, that makes the optimization considerably more complex, and this is not considered in this paper.

Once the individual optimal trajectories are found, the global problem is formulated by incorporating the constraints imposed by the telescoping requirements. The resulting problem becomes a

Received 20 December 2010; revision received 10 August 2011; accepted for publication 10 August 2011. Copyright © 2011 by the American Institute of Aeronautics and Astronautics, Inc. All rights reserved. Copies of this paper may be made for personal or internal use, on condition that the copier pay the \$10.00 per-copy fee to the Copyright Clearance Center, Inc., 222 Rosewood Drive, Danvers, MA 01923; include the code 0731-5090/12 and \$10.00 in correspondence with the CCC.

*Research Scientist; ekolemen@pppl.gov.

†Professor, Mechanical and Aerospace Department.

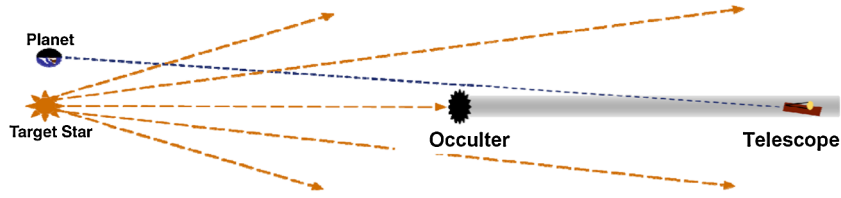


Fig. 1 Occluder-based extrasolar planet-finding mission diagram (data available at <http://newworlds.colorado.edu/starshade/index.htm>, retrieved 21 April 2011).

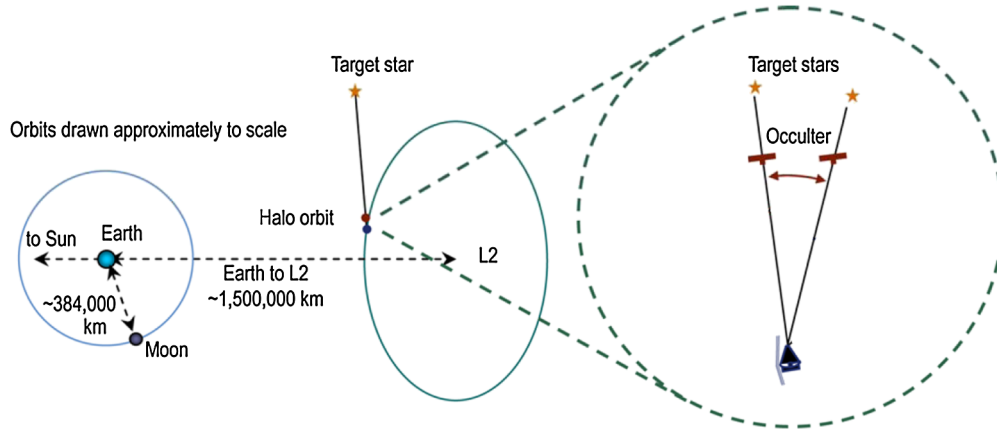


Fig. 2 Schematic diagram of occluder mission orbits projected onto the ecliptic plane [11].

dynamic time-dependent traveling salesman problem (TDTSP) with dynamical constraints. The simulated annealing and branching heuristic methods were used to solve it. The resulting global solution gives an approximate Delta-V budget for different configurations, which is useful for a trade study of various spacecraft control systems and strategies, as well as target selection.

For a concrete understanding of the feasibility of the mission, possible mission scenarios using current technology were investigated. To this end, possible missions with the capabilities of an example spacecraft, the Small Missions for Advanced Research in Technology (SMART-1), were simulated and analyzed. The number of star systems that can be imaged, the performance index used in this study, under different conditions is quantified and compared.

II. Finding the Optimal Trajectories

In this section, the optimal control of the realignment maneuver is examined, which entails finding the trajectory that takes the occluder from a given star LOS to another star LOS. The diffractive optics problem described in Vanderbei et al. [9] prescribes that the telescope and occluder separation be fixed for all observations. This fixes the position of the occluder to be on a sphere around the telescope, the specific location depending upon the chosen target star. The realignment problem then becomes one of finding an optimal trajectory between two two-dimensional surfaces (the initial separation from the previous observation and the new location for the next observation), as shown in Fig. 3. The scientific objective is to image the greatest number of star systems in the minimum amount of time. This objective leads to two possible optimizations. First, the optimization of the trajectories for minimum fuel consumption, which would increase the number of target stars that can be imaged with a given fuel budget. Second, finding the time-optimal trajectories that would allow imaging of the maximum number of stars in a given mission lifetime.

There are two approaches in use for trajectory optimization: the Euler-Lagrange formulation and direct optimization. Direct optimization simply discretizes the entire problem using appropriate numerical approximation techniques and then formulates a large nonlinear program. The Euler-Lagrange approach involves solving the two-point boundary value problem associated with an appropriate dynamic programming formulation. Both methods are

discussed, and examples are provided for each. Nevertheless, while the direct optimization can be more robust and is gaining favor, it involves much more computation. Since, for the global mission optimization, hundreds of thousands of these optimal trajectories must be found, computational efficiency is a major concern. Therefore, the Euler-Lagrange formulation was selected for the global optimization. Unfortunately, random initial conditions did not give convergent results for the Euler-Lagrange formulation of the minimum-fuel and minimum-time problem. Therefore, a stepwise approach for obtaining good initial guesses was adopted. First, the unconstrained minimum-energy problem was solved. While this is not the most physically meaningful of the cost functions, its quadratic nature makes it easier to solve and it provided good starting values for the other optimizations. Using the solution of this problem as an initial guess, the second, harder, more realistic problem was solved by adding a constraint on the maximum thrust. The solution of this problem gave sufficiently close initial guesses to solve the constrained minimum-fuel and minimum-time problems.

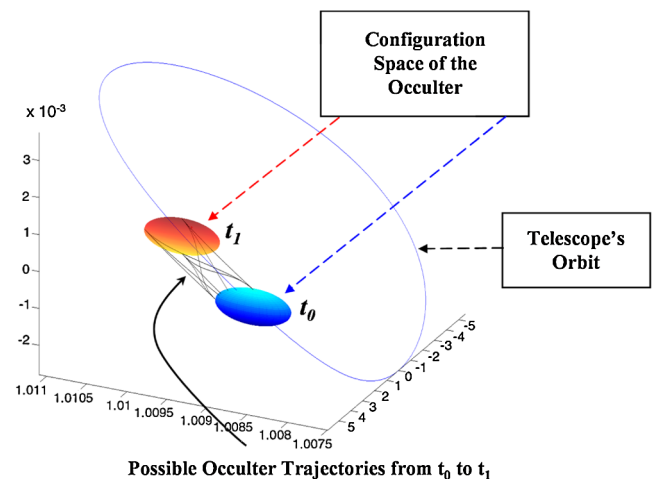


Fig. 3 Sphere of possible occluder locations about the telescope at two times and example optimal trajectories connecting them.

Depending on the type of thruster the mission uses, either continuous or discrete control might be needed. Since for this mission the most probable devices are Hall-type thrusters, which give access to continuous, low magnitude thrust throughout the trajectory, only the continuous thrust optimizations were studied. For all the control algorithms developed in this section, it is assumed that there is a single thruster that can be instantaneously aligned toward any direction of choice.

A. Problem Setup

The stars to be observed were taken from the list of the most suitable 100 stars for the terrestrial planet finder coronagraph (TPF-C) mission [12]. Then, the astrometrical data from the Hipparcos astronomical catalog [13] were used. The Naval Observatory Vector Astrometry Software routines developed by Kaplan et al. [14] were used to convert and update the exact star locations of the target stars relative to the solar system, starting arbitrarily from 1 January 2010. For high-fidelity simulations, the capability to use the full nonlinear solar system model based on the Jet Propulsion Laboratory DE-406 ephemeris [15] for differential equations was developed. However, in the analysis to follow, the circularly restricted three-body problem (CRTBP) simplified model is used for the dynamics, and a uniformly rotating star model is employed for the star locations for faster calculations.

During the imaging of a given planetary system, the telescope and the occulter must remain aligned to the LOS of the star position, requiring that the velocities of the telescope and occulter with respect to a reference frame aligned to the star be matched. For the time scales of interest, the stars are well approximated as stationary with respect to a frame fixed to the solar system barycenter (i.e., proper motion is ignored in this analysis). Thus, a barycentric inertial frame is defined located at the solar system barycenter with z axis perpendicular to the ecliptic, x axis pointed along the line of equinoxes, and y axis completing a right-hand set.

As mentioned, to simplify the dynamics, the CRTBP is used in which only the sun and the Earth as the two primaries are considered (with masses m_1 and m_2 , respectively), approximate their common orbit as circular, and treat the satellites (telescope and occulter) as massless. The rotating synodical frame R is defined to be located at the center of mass of the two primaries, with the z axis also perpendicular to the ecliptic and x axis along the sun–Earth line directed from m_1 to m_2 . The y axis completes the right-handed set. Normalizing the distances such that the distance between the primaries is 1, and normalizing time such that the period of the circular motion about the center of mass is 2π , the equations of motion of the state vector $\mathbf{x} = \{x, y, z, \dot{x}, \dot{y}, \dot{z}\}$ for either massless body can be written as

$$\dot{\mathbf{x}} = \mathbf{f}(\mathbf{x}) = \begin{pmatrix} \dot{x} \\ \dot{y} \\ \dot{z} \\ 2\dot{y} + \frac{\partial \bar{U}}{\partial x} + u_x \\ -2\dot{x} + \frac{\partial \bar{U}}{\partial y} + u_y \\ \frac{\partial \bar{U}}{\partial z} + u_z \end{pmatrix} \quad (1)$$

where $\mu = m_2/(m_1 + m_2)$; the shorthand notation $\dot{(\)}$ is used for the time derivative of a scalar; u_x , u_y , and u_z are the components of the thrust accelerations; and the effective potential $\bar{U}(x, y, z)$ is

$$\bar{U}(x, y, z) = \frac{1 - \mu}{\|\mathbf{r}_1\|} + \frac{\mu}{\|\mathbf{r}_2\|} + \frac{x^2 + y^2}{2} \quad (2)$$

For astronomically simplified models around sun–Earth L2, better results are obtained when the Earth/moon system is treated as a single planet with the center of mass at the Earth/moon barycenter than when the effect of the moon is ignored in the model. Thus, here, $\mu = 3.040423398444176 \times 10^{-6}$ constant for the (Earth/moon Barycenter)–sun system [16] was used with \mathbf{r}_1 , \mathbf{r}_2 as the position of the spacecraft with respect to the sun and the Earth–moon barycenter.

The CRTBP is characterized by a nonstiff and smooth set of ordinary differential equations. For nonstiff problems, an explicit numerical integration technique achieves the desired accuracy with minimal computational costs. Additionally, for smooth ordinary differential equations (ODEs), higher-order integration methods can be employed, which further reduces the computation time. Thus, to numerically propagate the initial state variables, an explicit seventh-order Runge–Kutta method was used. The method integrates a system of ODEs using seventh-order Dormand and Prince formulas [17] and uses the eighth-order results for adapting the step size.

For ease of comparison, all the missions scenarios discussed assume a base halo orbit around L2 with an out-of-plane amplitude of 500,000 km.

B. Optimal Control Problem Formulation

The optimal control problem is to find the time history of the controls $u_x(t)$, $u_y(t)$, and $u_z(t)$ during a transfer to minimize some performance index: in our case, either fuel use or time. As described in the Introduction, two standard computational techniques are employed: The Euler–Lagrange (indirect) method or the SQP (direct) approach. The Euler–Lagrange approach is described thoroughly in Bryson and Ho [18]. It finds the optimal trajectory $\mathbf{x}(t)$ and control $\mathbf{u}(t)$ that minimizes an integral cost on the state and control subject to the constraints that they satisfy the equations of motion in Eq. (1). The final trajectories for the state and adjoint are given as the solution of a two-point boundary value problem. The main advantage of using the Euler–Lagrange formulation is that the optimality of the solution can be checked, and the computational effort for solving the boundary value problem (BVP) using shooting or collocation methods will be minimal if a feasible solution can be found. The main disadvantage of this formulation is that it may be difficult to generate sufficiently good initial guesses for the adjoint states to ensure convergence to even a local solution.

The second approach to solving the optimization problem is to discretize the integral cost and the trajectory and solve a high-dimensional nonlinear optimization problem via an appropriate nonlinear optimization algorithm. Since there are no intermediate steps, such as the introduction of the adjoint state, involved in solving the problem, numerical methods that employ nonlinear programming algorithms to solve the discretized optimal control problem are called direct. An overview of direct methods is given in Gill et al. [19] and references therein. One of the most efficient and promising methods currently in use is the SQP algorithm. The SQP algorithm is a generalization of Newton’s method for unconstrained optimization in that it finds a step away from the current point by minimizing a quadratic model of the problem. The SQP algorithm replaces the objective function with a quadratic approximation and replaces the constraint functions by linear approximations. A more detailed overview of the SQP method can be found at Gill et al. [19].

IPOPT [20], an open-source interior point method SQP-solver software, was used in this study. To minimize the time it takes to convert the optimal control problem to a form that can be used with the direct method, an automated symbolic software was created. This algorithm discretizes the optimal control problem, which is defined effortlessly in MATLAB. It then symbolically converts the problem to the form needed by the SQP solver. This code is then converted and compiled in FORTRAN, which is much faster than MATLAB. These compiled functions are in a form that can be called from within a MATLAB script (see MATLAB’s “mex” utility for more information). This enables solving the problem without leaving the convenience of the MATLAB environment while benefiting from the speed of the FORTRAN’s fast compiler. The software allows for a choice between many different discretization methods, such as Runge–Kutta, Euler, and trapezoidal, in order to suit the needs of the specific problem.

[‡]Data available at <http://www.mathworks.com/support/tech-notes/1600/1605.html> [retrieved 5 January 2007].

C. Optimization of the Realignment Maneuver

In this section, both optimization approaches to find both the minimum-fuel and minimum-time trajectories and control for a single realignment maneuver are used. Unfortunately, it was observed that starting with no prior knowledge resulted in both problems being infeasible; it was necessary to use another technique to find trajectories close to the optimal ones. Therefore, first, the easier unconstrained and constrained minimum-energy problems were solved to find initial guesses for the minimum-time and minimum-fuel optimizations.

In every case, it is assumed that the control variable is the acceleration of the spacecraft due to the force applied by the thrusters throughout its trajectory $\mathbf{u} = (d^2\mathbf{x}/dt^2)_{\text{thruster}}$. Then, the effect of the control can be added to the normal control-free Newtonian equations such that

$$\dot{\mathbf{x}} = \mathbf{f}_{\text{ctr}}(t, \mathbf{x}, \mathbf{u}) \quad (3)$$

where

$$\mathbf{f}_{\text{ctr}}(t, \mathbf{x}, \mathbf{u}) = \mathbf{f}(t, \mathbf{x}) + \{0, 0, 0, u_x, u_y, u_z\}^T \quad (4)$$

and where the control vector \mathbf{u} is defined as $\mathbf{u} = \{u_x, u_y, u_z\}^T$.

1. Unconstrained Minimum-Energy Optimization

In the minimum-energy optimization, our aim is to minimize a quadratic integral of the control effort

$$J = \int_{t_0}^{t_f} \frac{1}{2} \mathbf{u}^T \mathbf{u} dt \quad (5)$$

While this is not the most physically meaningful of the cost functions, because it is quadratic, it is easier to solve and is thus useful for finding starting values for the other optimizations. The Hamiltonian for this optimal control problem is

$$H(t, \mathbf{x}, \boldsymbol{\lambda}, \mathbf{u}) = \frac{1}{2} \mathbf{u} \cdot \mathbf{u} + \boldsymbol{\lambda}^T \mathbf{f}(t, \mathbf{x}) + \mathbf{p}^T \mathbf{u} \quad (6)$$

where $\boldsymbol{\lambda} = \{\lambda_1, \lambda_2, \lambda_3, \lambda_4, \lambda_5, \lambda_6\}^T$ is the adjoint vector, and the intermediate variable \mathbf{p} is the last three elements of the adjoint vector $\mathbf{p} = \{\lambda_4, \lambda_5, \lambda_6\}^T$ (see Bryson and Ho [18] for details of the Euler-Lagrange formulation).

In this section, the point-to-point optimal control is considered, where both the initial and final states are fixed a priori:

$$\psi(t_f) = \mathbf{x}(t_f) - \mathbf{x}_f = 0 \quad (7)$$

Solving the optimality condition

$$\mathbf{0} = \frac{\partial H(t, \mathbf{x}, \boldsymbol{\lambda}, \mathbf{u})}{\partial \mathbf{u}} \quad (8)$$

the control is obtained as follows:

$$\mathbf{u} = -\mathbf{p} \quad (9)$$

Substituting for \mathbf{u} in the Euler-Lagrange equations, a 12 state ODE in terms of the state and adjoint state only is obtained:

$$\dot{\mathbf{x}} = \mathbf{f}(t, \mathbf{x}, \boldsymbol{\lambda}), \quad \dot{\boldsymbol{\lambda}} = -\left(\frac{\partial \mathbf{f}(t, \mathbf{x}, \boldsymbol{\lambda})}{\partial \mathbf{x}}\right)^T \boldsymbol{\lambda} \quad (10)$$

with the 12 boundary conditions

$$\begin{pmatrix} \mathbf{x}(t_0) - \mathbf{x}_0 \\ \mathbf{x}(t_f) - \mathbf{x}_f \end{pmatrix} = \mathbf{0} \quad (11)$$

the problem becomes a BVP. This problem is solved with collocation where the differential equation part is converted to discrete relationships along the trajectory via Simpson's formula for the quadrature, and then these constraints are augmented with boundary conditions. The resulting high-dimensional nonlinear equation is solved using Newton's method, following Kierzenka and Shampine's *bvp4c*

implementation [21]. The same collocation method is used throughout this paper.

To make sure that this solution is indeed an optimal solution of the problem, it is checked that the Legendre-Clebsch and Weierstrass conditions are satisfied:

$$\frac{\partial^2 H(t, \mathbf{x}, \mathbf{u}, \boldsymbol{\lambda})}{\partial \mathbf{u}^2} = I > 0 \quad (12)$$

For the case of transfer from a star LOS to another, the occulter-to-telescope distance R of 50,000 km is used. The time of flight is chosen to be two weeks, which is a representative slew time for the mission under study. It is assumed that the telescope is on a halo orbit and that the first star the occulter-telescope formation looks at is in the direction given by the unit vector $\hat{\mathbf{e}}_0$, while the second star to be imaged is in the direction of the unit vector $\hat{\mathbf{e}}_1$. The exact numerical values used in the example to follow are

$$\hat{\mathbf{e}}_0 = \begin{pmatrix} 6.324555320336759 \times 10^{-1} \\ -6.324555320336759 \times 10^{-1} \\ 4.472135954999580 \times 10^{-1} \end{pmatrix}, \quad \hat{\mathbf{e}}_1 = \begin{pmatrix} 0 \\ 0 \\ 1 \end{pmatrix} \quad (13)$$

so that the angle between the unit vector is 63 deg. The target star and occulter positions are obtained from the unit vectors as

$$\mathbf{r}_{\text{occ}} = \mathbf{r}_{\text{tel}} + R\hat{\mathbf{e}} \quad (14)$$

where \mathbf{r}_{occ} and \mathbf{r}_{tel} are the position of the occulter and the telescope with respect to the synodical frame origin, respectively. The velocities are obtained based on the requirement that the inertial velocities of both the telescope and the occulter be the same:

$$\mathbf{v}_{\text{occ}} = \mathbf{v}_{\text{tel}} + \boldsymbol{\omega} \times R\hat{\mathbf{e}} \quad (15)$$

where \mathbf{v}_{occ} and \mathbf{v}_{tel} are the velocity of the occulter and the telescope in the synodical frame, respectively, and $\boldsymbol{\omega} = \{0, 0, 1\}^T$ is the angular velocity of the CTRBP. Thus, the numerical values in the normalized synodical units for the BVP algorithm are

$$\mathbf{x}_0 = \begin{pmatrix} 1.008708480181499 \times 10^0 \\ 5.219658053604695 \times 10^{-3} \\ 1.494719120781122 \times 10^{-4} \\ 3.123278717913480 \times 10^{-3} \\ 2.077725728577118 \times 10^{-3} \\ 6.483432393011172 \times 10^{-3} \end{pmatrix} \quad \mathbf{x}_f = \begin{pmatrix} 1.009397510830226 \times 10^0 \\ 5.341370714348193 \times 10^{-3} \\ 1.843136365772625 \times 10^{-3} \\ 3.951895067977367 \times 10^{-3} \\ -2.937081366176431 \times 10^{-3} \\ 5.838803068471303 \times 10^{-3} \end{pmatrix} \quad (16)$$

Figure 4 shows the optimal trajectory of the occulter relative to the telescope on the halo orbit. Figure 5 shows the optimal control throughout the trajectory. In the figure, the magnitude of control is shown on the left and the components obtained via direct and indirect methods are shown on the right. In the figure, the line is the Euler-Lagrange BVP solution, while the black crosses are the direction solution. Both solutions are in general agreement; the BVP solution is more accurate because of the finer grid resolution.

2. Constrained Minimum-Energy Optimization

Next, the minimum-energy problem is refined by constraining the maximum control force available. Apart from the different cost function, the constrained minimum-energy problem is mathematically the same as the time and fuel optimization problems. This

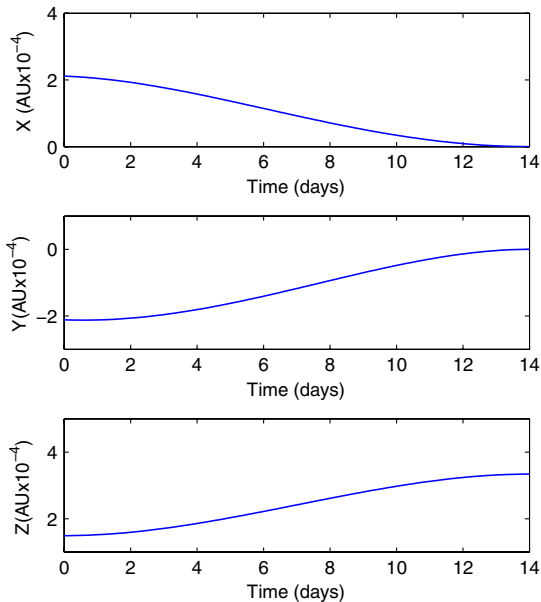


Fig. 4 Trajectory of the occulter relative to the telescope for an energy-optimal realignment maneuver.

similarity enables the solution of this problem to be used as the initial guess for the time and fuel optimization problems described in the following two sections.

The magnitude of the control vector $|\mathbf{u}|$ is constrained to be less than a specified limit u_{\max} , such that $|\mathbf{u}| < u_{\max}$. The augmented Hamiltonian for the optimal control problem can be written as

$$H_{\text{aug}}(t, \mathbf{x}, \boldsymbol{\lambda}, \mathbf{u}) = \frac{1}{2} \mathbf{u}^T \mathbf{u} + \boldsymbol{\lambda}^T \mathbf{f}(t, \mathbf{x}) + \mathbf{p}^T \mathbf{u} + \mu_{\text{eff}} c_{\text{eff}}(\mathbf{u}) \begin{cases} \mu_{\text{eff}} = 0 & \text{if } c_{\text{eff}}(\mathbf{u}) < 0 \\ \mu_{\text{eff}} \geq 0 & \text{if } c_{\text{eff}}(\mathbf{u}) = 0 \end{cases} \quad (17)$$

where $c_{\text{eff}}(\mathbf{u})$ is the inequality constraint function effective on the boundary

$$c_{\text{eff}}(\mathbf{u}) = \mathbf{u}^T \mathbf{u} - u_{\max}^2 \leq 0 \quad (18)$$

and μ_{eff} is the corresponding Lagrange multiplier.

Since c_{eff} is only a function of \mathbf{u} , the adjoint differential equations are not altered. However, the condition for control optimality becomes

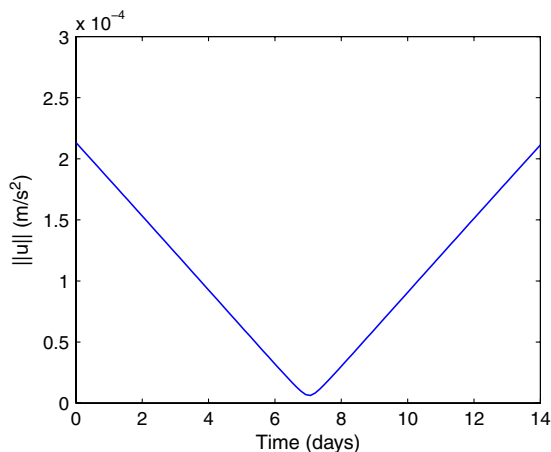


Fig. 5 Optimal minimum-energy control effort for the realignment maneuver shown in Fig. 4.

$$\mathbf{0} = \frac{\partial H^T}{\partial \mathbf{u}} = \begin{cases} \mathbf{u} + \mathbf{p}, & c_{\text{eff}} < 0 \\ \mathbf{u} + \mathbf{p} + 2\mu_{\text{eff}} \mathbf{u}, & c_{\text{eff}} = 0 \end{cases} \quad (19)$$

Solving the first part of the equation gives $\mathbf{u} = -\mathbf{p}$, as before. The second part asks that the following two equations be satisfied:

$$\mathbf{u} = -\frac{\mathbf{p}}{1 + 2\mu_{\text{eff}}} \quad \text{and} \quad |\mathbf{u}| = u_{\max} \quad (20)$$

which are solved to give

$$\mathbf{u} = \pm u_{\max} \frac{\mathbf{p}}{|\mathbf{p}|} \quad (21)$$

To decide which sign the control should take, the Pontryagin's minimum principle (See Kirk for details [22]) is used, which states that the optimal control \mathbf{u}^* in the set of feasible controls \mathcal{U} is

$$\mathbf{u}^*(t) = \arg\{\min_{\mathbf{u}(t) \in \mathcal{U}} H(t, \mathbf{x}, \mathbf{u}, \boldsymbol{\lambda})\} \quad (22)$$

Looking at the part of the Hamiltonian with control influence, the following inequality is obtained:

$$\frac{1}{2} \mathbf{u}^{*T} \mathbf{u}^* + \mathbf{p}^{*T} \mathbf{u}^* \leq \frac{1}{2} \mathbf{u}^T \mathbf{u} + \mathbf{p}^{*T} \mathbf{u} \quad (23)$$

where the superscript $\{*\}$ denotes the optimal elements. Now it becomes apparent that the correct choice of the sign is minus. This defines the optimal control as

$$\mathbf{u} = \begin{cases} -\mathbf{p} & \text{if } |\mathbf{p}| \leq u_{\max} \\ -u_{\max} \frac{\mathbf{p}}{|\mathbf{p}|} & \text{if } |\mathbf{p}| > u_{\max} \end{cases} \quad (24)$$

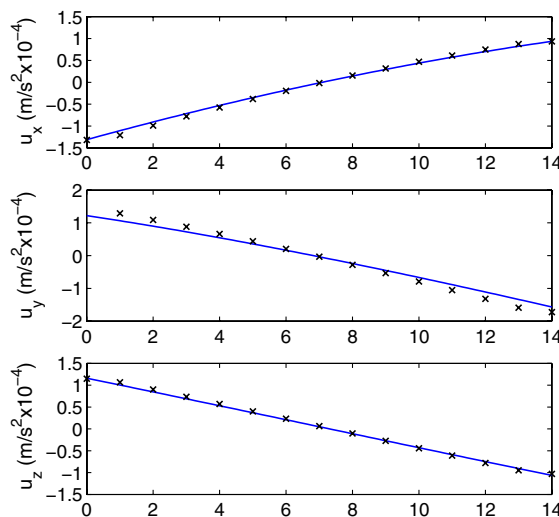
Substituting for \mathbf{u} in the Euler Lagrange equations, a 12 deg ODE is obtained in terms of the state and adjoint state only:

$$\dot{\mathbf{x}} = \mathbf{f}(t, \mathbf{x}, \boldsymbol{\lambda}) \quad \dot{\boldsymbol{\lambda}} = -\left(\frac{\partial \mathbf{f}(t, \mathbf{x}, \boldsymbol{\lambda})}{\partial \mathbf{x}}\right)^T \boldsymbol{\lambda} \quad (25)$$

with boundary conditions

$$\begin{pmatrix} \mathbf{x}(t_0) - \mathbf{x}_0 \\ \mathbf{x}(t_f) - \mathbf{x}_f \end{pmatrix} = \mathbf{0} \quad (26)$$

While solving the constrained optimization problem for the realignment maneuver, the same \mathbf{x}_0 and \mathbf{x}_f given in Eq. (16) in the last section are used, and the initial guess for the BVP is set to the solutions from the last section. Figure 6 shows the magnitude and the components of the optimal control history throughout the trajectory for an example thrust constrained optimization. In the figure, the



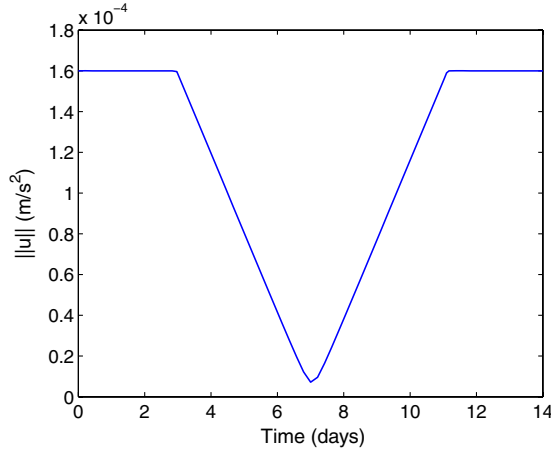


Fig. 6 Example of optimal minimum-energy control with thrust constrained to $1.6 \times 10^{-4} \text{ m/s}^2$.

magnitude of control is shown on the left and the components obtained via direct and indirect methods are shown on the right. In the figure, the line is the Euler–Lagrange BVP solution, while the black crosses are the direct solution. Both solutions are in general agreement. In this example, u_{\max} is set to $1.6 \times 10^{-4} \text{ m/s}^2$.

3. Minimum-Time Optimization

Now the realignment between two targets in minimum time under a maximum thrust constraint is considered. In this case, the aim is to go from a point in phase space to another point in the minimum amount of time. The cost function thus becomes

$$J = \int_{t_0}^{t_f} 1 \, dt \quad (27)$$

Since the minimum-time solution dictates that the maximum control be employed at all times, the problem is simplified by redefining the control:

$$\mathbf{u} = u_{\max} \hat{\mathbf{u}} \quad (28)$$

Now there is a new constraint that needs to be satisfied throughout the trajectory:

$$\hat{\mathbf{u}}^T \hat{\mathbf{u}} = 1 \quad (29)$$

This constraint is included in the Hamiltonian by augmenting it with additional Lagrange multipliers μ :

$$H = 1 + \lambda^T \mathbf{f}(\mathbf{x}) + u_{\max} \mathbf{p}^T \hat{\mathbf{u}} + \mu (\hat{\mathbf{u}}^T \hat{\mathbf{u}} - 1) \quad (30)$$

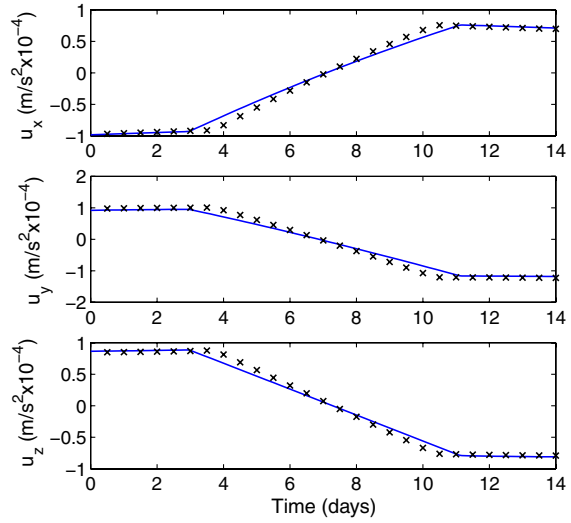
While the augmentation does not affect the adjoint differential equation, the optimality condition becomes

$$0 = \frac{\partial H}{\partial \hat{\mathbf{u}}} = u_{\max} \mathbf{p} + \mu \hat{\mathbf{u}} \quad (31)$$

Thus, the optimal control $\hat{\mathbf{u}}$ can be obtained by solving this equation along with constraint equation (29):

$$\mathbf{u} = \begin{cases} -u_{\max} \frac{\mathbf{p}}{|\mathbf{p}|} & \text{if } |\mathbf{p}| \neq 0 \\ \text{undetermined} & \text{if } \mathbf{p} = \mathbf{0} \end{cases} \quad (32)$$

Previously, the optimality condition and Pontryagin's minimum principle were used to determine $\mathbf{u}^*(t)$ for all time $t \in [t_0, t_f]$ in terms of the extremal states \mathbf{x}^* and adjoint states λ^* . If, however, there is a time interval $[t_1, t_2]$ of finite duration during which this principle provides no information about the optimal control, then the problem is called singular and the interval $[t_1, t_2]$ is called the singular interval.



To determine whether it is possible to have singular intervals, the case where \mathbf{p} is zero for a finite time interval is considered. This condition implies that derivatives of all orders of \mathbf{p} should be zero during that time interval. In other words,

$$\frac{d^k \mathbf{p}}{dt^k} = 0 \quad k = 1, 2, \dots \quad (33)$$

Writing the differential equation for \mathbf{p} from the adjoint states ODE,

$$\dot{\mathbf{p}} = \begin{pmatrix} -\lambda_1 + 2p_2 \\ -\lambda_2 - 2p_1 \\ -\lambda_3 \end{pmatrix} \quad (34)$$

it is observed that the singularity condition leads to $\lambda = 0$. However, for the open-end-time problem under study, there is another boundary condition. The Hamiltonian for the open-end-time problems, where it is not an explicit function of time, is equal to zero at all times (see Stengel [23] for details). Therefore, for the CRTBP where H is not an explicit function of time,

$$H = 0 \quad (35)$$

For the singular intervals, $\lambda = \mathbf{0}$. Substituting this equality in the Hamiltonian, $H = 1$ is obtained, which leads to a contradiction. Thus, there cannot be singular intervals for this minimum-time optimization problem.

Substituting for $\hat{\mathbf{u}}$ in the Euler–Lagrange equations, a 12 deg ODE in terms of the state and adjoint state only is obtained:

$$\dot{\mathbf{x}} = \mathbf{f}(t, \mathbf{x}, \lambda) \quad \dot{\lambda} = - \left(\frac{\partial \mathbf{f}(\mathbf{x}, \lambda)}{\partial \mathbf{x}} \right)^T \lambda \quad (36)$$

with boundary conditions

$$\begin{pmatrix} H \\ \mathbf{x}(t_0) - \mathbf{x}_0 \\ \mathbf{x}(t_f) - \mathbf{x}_f \end{pmatrix} = \mathbf{0} \quad (37)$$

To apply numerical methods to solve this problem, the time boundaries for the BVP must be defined explicitly. However, in this case, the time interval is $[0, t_f]$, where the end time for the BVP t_f is an unknown parameter. To overcome this problem, the system is redefined on the fixed-time interval $[0, 1]$ by rewriting the equation in terms of a new time variable:

$$\tau = \frac{t}{t_f} \quad (38)$$

Introducing t_f as a new state variable, the extended differential equation becomes

$$\frac{d\mathbf{x}}{d\tau} = t_f \mathbf{f}(\tau, \mathbf{x}, \mathbf{u}) \quad \frac{d\boldsymbol{\lambda}}{d\tau} = -t_f \left(\frac{\partial \mathbf{f}(\tau, \mathbf{x}, \boldsymbol{\lambda})}{\partial \mathbf{x}} \right)^T \boldsymbol{\lambda} \quad \frac{dt_f}{d\tau} = 0 \quad (39)$$

Now the 13-dimensional BVP can be solved.

The requirement for realignment is that, at the final time, the occulter must be positioned to look at a prespecified star with the inertial direction $\hat{\mathbf{e}}$. Recall that, at different times, the position and velocity of the occulter are given by

$$\mathbf{r}_{\text{occ}} = \mathbf{r}_{\text{tel}} + R\hat{\mathbf{e}} \quad (40)$$

$$\mathbf{v}_{\text{occ}} = \mathbf{v}_{\text{tel}} + \boldsymbol{\omega} \times R\hat{\mathbf{e}} \quad (41)$$

Thus, before knowing the time to go, the position of the telescope and, as a consequence, the final position of the occulter \mathbf{x}_f cannot be specified. This problem can be solved in two ways. The first option is to change the time-independent final time constraint to

$$\psi(t_f) = \boldsymbol{\epsilon}^T \boldsymbol{\epsilon} \quad \text{where } \boldsymbol{\epsilon} = \begin{pmatrix} \mathbf{r}_{\text{occ}} - (\mathbf{r}_{\text{tel}} + R\hat{\mathbf{e}}) \\ \mathbf{v}_{\text{occ}} - (\mathbf{v}_{\text{tel}} + \boldsymbol{\omega} \times R\hat{\mathbf{e}}) \end{pmatrix} \quad (42)$$

This changes the 13th boundary condition $H(t_f) = 0$ to

$$H(t_f) + \frac{\partial \psi(t_f)}{\partial t} = 0 \quad (43)$$

However, due to the time-dependent nature of the boundary condition, it is difficult to solve this BVP. Instead, an iterated approach to solving the target-chasing minimum-time problem is employed. First, the t_f is estimated and then the equations of motion are integrated to find the location of the telescope and the star at that time. From the LOS requirement, \mathbf{x}_f is obtained and then the time-independent version of the problem is solved. After obtaining the minimum time to go, \mathbf{x}_f is calculated and the optimization is repeated with the new final position constraint. The iteration continued until the difference between the estimate and the t_f from the optimization was negligible. In this case, two to three iterations were adequate. Figure 7 shows the time-optimal trajectories for three scenarios and the control components for one of them. In the figure, the light gray line is the Euler–Lagrange BVP solution, while the black crosses are

the direct solution. The direct method finds smaller time-to-go values due to its higher resolution.

4. Minimum-Fuel Optimization

In the fuel-optimal problem, the aim is to find the control history that takes the spacecraft to the predefined final position in a given time t_f while keeping the final mass $m(t_f)$ as high as possible. The mass of a spacecraft at a given time t can be determined by the relationship

$$m(t) = m_0 - \dot{m}t \quad (44)$$

where \dot{m} is the constant propellant flow rate and m_0 is the mass of the spacecraft at the initial time. Assuming that the total change in the mass throughout the trajectory is negligible, Newton’s second law of motion can be written as

$$|\mathbf{u}|m_0 \approx \dot{m}V_{\text{ex}/b} \quad (45)$$

and it follows that

$$m(t_f) \approx m_0 \left(1 - \frac{t_f |\mathbf{u}|}{V_{\text{ex}/b}} \right) \quad (46)$$

where $V_{\text{ex}/b}$ is the velocity of exhaust with respect to the body and \mathbf{u} is the inertial acceleration due to spacecraft propulsion: the control input that has been used throughout this section. The velocity of the exhaust depends on the specifications of the spacecraft thruster.

The constant mass approximation is a very good one for the LOS realignment maneuver since such maneuvers take at most a few weeks. With this approximation, maximizing final mass is equivalent to minimizing the magnitude of the control throughout the trajectory. For this case, the cost function is

$$J = \int_{t_0}^{t_f} |\mathbf{u}| dt \quad (47)$$

The Hamiltonian for the control problem becomes

$$H(t, \mathbf{x}, \boldsymbol{\lambda}, \mathbf{u}) = |\mathbf{u}| + \boldsymbol{\lambda}^T \mathbf{f}(t, \mathbf{x}) + \mathbf{p}^T \mathbf{u} \quad (48)$$

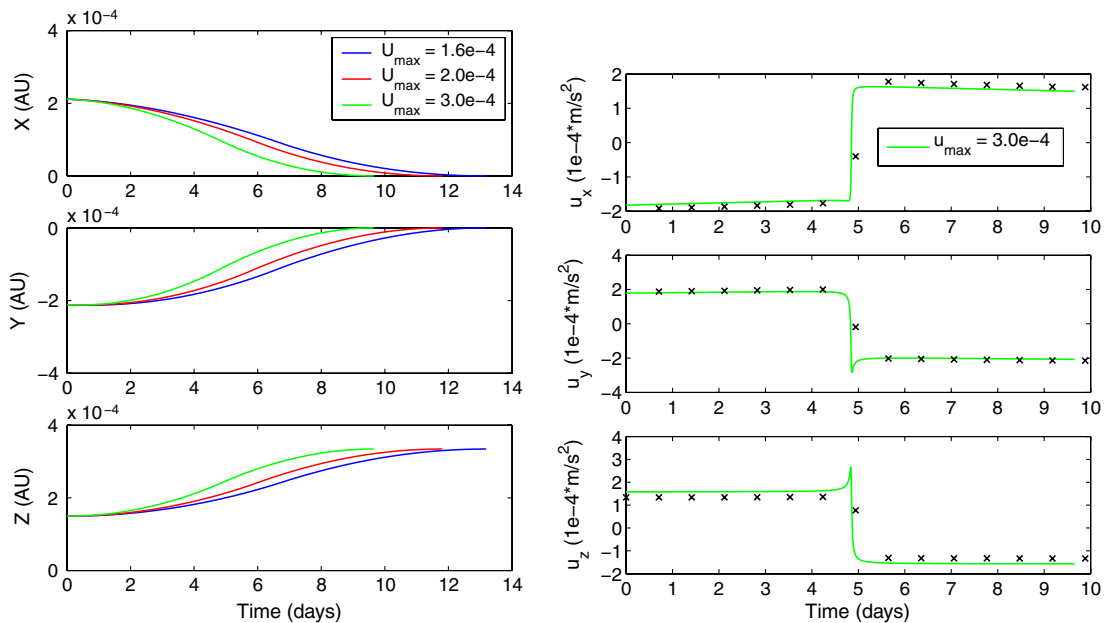


Fig. 7 Sample of trajectories of occulter relative to the telescope for the time-optimal control for different u_{max} (left). Components of an example time-optimal control with thrust constrained to $3.0 \times 10^{-4} \text{ m/s}^2$ obtained via direct and indirect methods, shown with solid lines and black crosses, respectively (right).

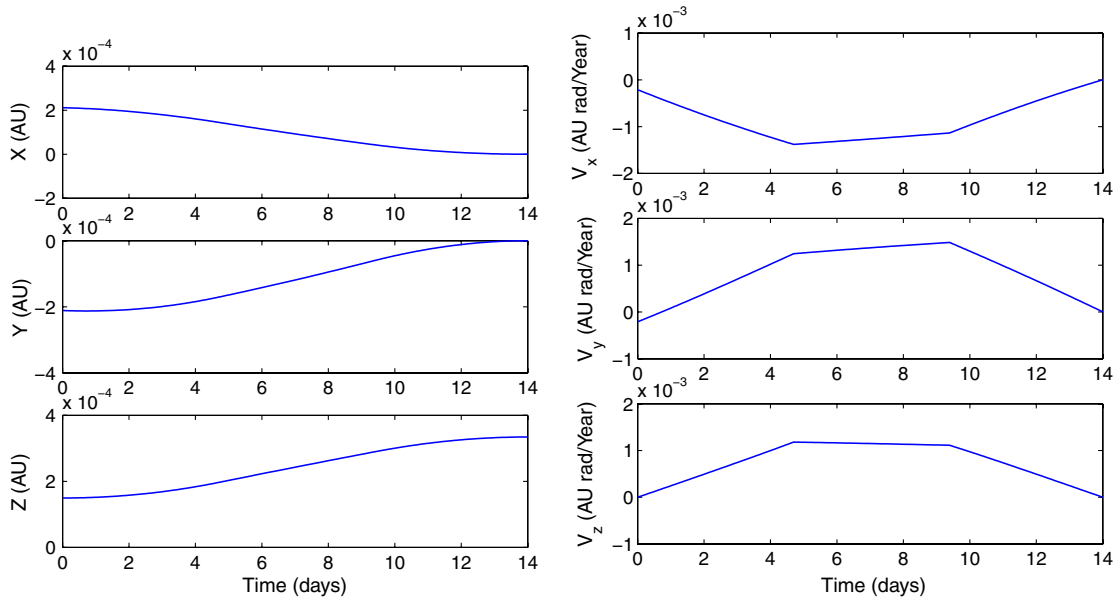


Fig. 8 Trajectory of the occulter relative to the telescope for a minimum-fuel realignment maneuver.

Pontryagin's minimum principle states that the optimal control is

$$\mathbf{u}^*(t) = \arg\{\min_{\mathbf{u}(t) \in \mathcal{U}} H(t, \mathbf{x}, \mathbf{u}, \boldsymbol{\lambda})\} \quad (49)$$

Looking at the part of the Hamiltonian with control influence, the following inequality is obtained:

$$|\mathbf{u}^*| + \mathbf{p}^{*T} \mathbf{u}^* \leq |\mathbf{u}| + \mathbf{p}^{*T} \mathbf{u} \quad (50)$$

where the superscript $\{*\}$ denotes the optimal elements. Along with the inequality constraint $|\mathbf{u}| < u_{\max}$, the optimal control is obtained as

$$\mathbf{u} = \begin{cases} \mathbf{0} & \text{if } |\mathbf{p}| < 1 \\ -u_{\max} \frac{\mathbf{p}}{|\mathbf{p}|} & \text{if } |\mathbf{p}| > 1 \\ \text{undetermined} & \text{if } |\mathbf{p}| = 1 \end{cases} \quad (51)$$

It is important to now determine whether the undetermined case leads to singular control. To prove or disprove whether singular control exists in the nonlinear case is very difficult. Therefore, the linear case is studied in order to gain insight into the nonlinear solution.

To prove that no singular control intervals exist for the realignment maneuver, differential equation (1) is linearized to

$$\dot{\mathbf{x}} = \mathbf{A}\mathbf{x} + \mathbf{B}\mathbf{u} \quad (52)$$

For this problem, it can be shown that \mathbf{A} is nonsingular and that the controllability matrix

$$\mathcal{C} = [\mathbf{B} \quad \mathbf{A}\mathbf{B} \quad \mathbf{A}^2\mathbf{B} \quad \dots \quad \mathbf{A}^{n-1}\mathbf{B}] \quad (53)$$

where n is the dimension of the system, is of full rank n . It is known that, for a nonsingular system with complete controllability, the system does not have singular solutions (see Kirk [22] for details). Thus, the control law for the linearized system does not have singular arcs and is given by

$$\mathbf{u} = \begin{cases} \mathbf{0} & \text{if } |\mathbf{p}| < 1 \\ -u_{\max} \frac{\mathbf{p}}{|\mathbf{p}|} & \text{if } |\mathbf{p}| \geq 1 \end{cases} \quad (54)$$

Next, the Euler-Lagrange solution to the optimal control problem is derived assuming that the linear analysis extends to the nonlinear case. Following this derivation, these results are compared with the direct method, which does not make any assumption about singularity, and it is shown that the results match numerically. Thus, it is concluded that the nonsingularity assumption is correct based on the linear analysis and numerical comparison.

Substituting for \mathbf{u} in the Euler-Lagrange equations, a 12 deg ODE is obtained in terms of the state and adjoint state only:

$$\dot{\mathbf{x}} = \mathbf{f}(t, \mathbf{x}, \boldsymbol{\lambda}) \quad \dot{\boldsymbol{\lambda}} = -\left(\frac{\partial \mathbf{f}(\mathbf{x}, \boldsymbol{\lambda})}{\partial \mathbf{x}}\right)^T \boldsymbol{\lambda} \quad (55)$$

with boundary conditions

$$\begin{pmatrix} \mathbf{x}(t_0) - \mathbf{x}_0 \\ \mathbf{x}(t_f) - \mathbf{x}_f \end{pmatrix} = \mathbf{0} \quad (56)$$

For the slew from one target to another, a backward shooting approach is obtained. Good initial conditions are crucial for the shooting method based on the Euler-Lagrange equations. The solution from the constrained minimum-energy optimization section is used as the initial guess for the adjoint variables at final time λ_f . Integrating the 12-dimensional differential equation, the root-finding problem becomes:

$$\boldsymbol{\phi}(t_0 - t_f, [\mathbf{x}_f; \boldsymbol{\lambda}_f]) - \mathbf{x}_0 = \mathbf{0} \quad (57)$$

Successive iteration gives the value of the λ_f in a few iterations. Figure 8 shows a sample fuel-optimal trajectory, where the relative trajectory of the occulter with respect to the telescope on the halo orbit is plotted. The bang-off-bang structure for the $J = \int |\mathbf{u}|$ type of optimization can be seen in Fig. 9, where the magnitude and the components of the control effort for the realignment maneuver are shown. Figure 9 also shows that the direct method, which does not make any assumptions about singularity, gives the same result as the indirect method. Thus, it is concluded that optimal control is nonsingular.

D. Result: Trajectory Optimization for SMART-1 as an Occulter

In this section, a specific spacecraft, SMART-1, is used to compute example minimum-fuel and minimum-time trajectories. Designed by ESA to test continuous solar-powered ion thrusters, SMART-1 successfully left the gravitational field of Earth and reached the mission objective of impacting the moon.[§] SMART-1 was chosen for a feasibility test because its solar-powered Hall-effect thrusters may be good candidates for the occulter-based telescopic mission under study. Using the characteristics of the SMART-1 thrusters [24] (see Table 1), the optimal trajectories between every pair of the top 100 TPF-C target stars were computed.

[§]Data available at <http://www.esa.int/SPECIALS/SMART-1> [retrieved 5 January 2007].

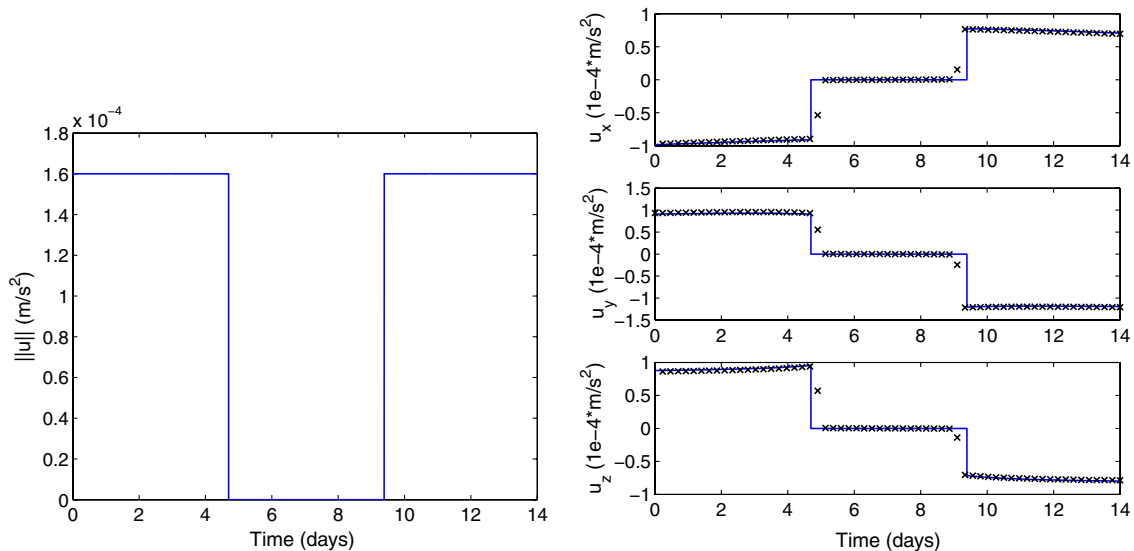


Fig. 9 Minimum-fuel control effort for the realignment maneuver shown in Fig. 8 (left: magnitude of control; right: components obtained via direct and indirect methods, shown on with solid lines and black crosses, respectively).

The minimum realignment time between targets assuming the maximum thrust capability of SMART-1 can be obtained for any specific time of year and position of the telescope on the halo orbit. An example minimum-time surface is shown in Fig. 10. It shows that, for the chosen SMART-1 thrusters and mass of the occulter, most transfers occur in under two weeks. In Sec. III, these minimum-time results are used to construct observing paths for given mission lengths.

A surface of minimum-fuel trajectories for given transfer times can also be obtained. Based on the minimum-time results, the transfer time is fixed to two weeks and, similarly, minimum-fuel trajectories between every pair of target stars are computed. An example minimum-fuel surface is shown in Fig. 11, where total Delta-V is used as a surrogate for total fuel consumption. For the sake of reasonable display, the unreachable targets (that is, targets that cannot be reached in two weeks even at full thrust) are shown with a Delta-V of zero as opposed to infinity. Thus, the two regions in the lower right and upper left corners, shown in black, represent targets that cannot be reached within two weeks.

These two surfaces of minimum-time trajectories and minimum-fuel trajectories provide a means for globally optimizing the mission. By treating them as graphs, the optimal ordering of observations that minimizes either the total mission length or the total fuel used for a given number of observations can be investigated. This is a variant of the traveling salesmen problem (TSP), which allows application of the known solution approaches. In the next section, it is shown how to formulate the appropriate TSP and solve it for various optimal mission scenarios that maximize the number of scientific observations for a given mission length or fuel supply.

III. Global Optimization of the Mission: The Traveling Salesman Problem

In this section, the previous optimal trajectory results are used to study approaches for globally optimizing different occulter-based

Table 1 Specifications of the SMART-1 spacecraft

Parameter	Value
Maximum thrust	68 mN
Mass ratio	0.83
Propellant mass	80 kg
Total Delta-V	3900 m/s
I_{sp}	1640 s
Maximum acceleration	0.2 mm/s ²
Full thrust lifetime	210 days

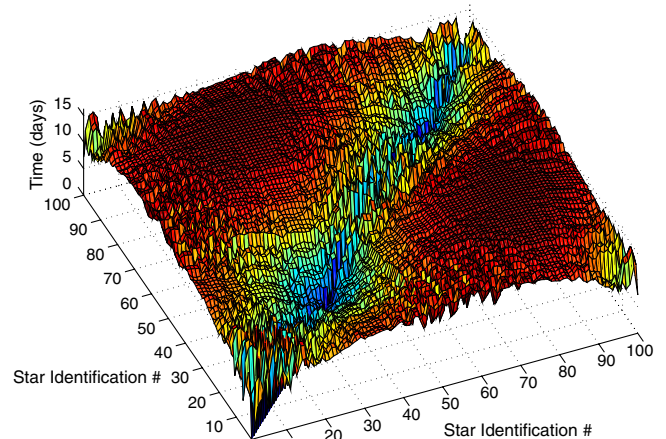


Fig. 10 Minimum time to realign between top 100 TPF-C targets with SMART-1 capabilities ($R = 50,000$ km).

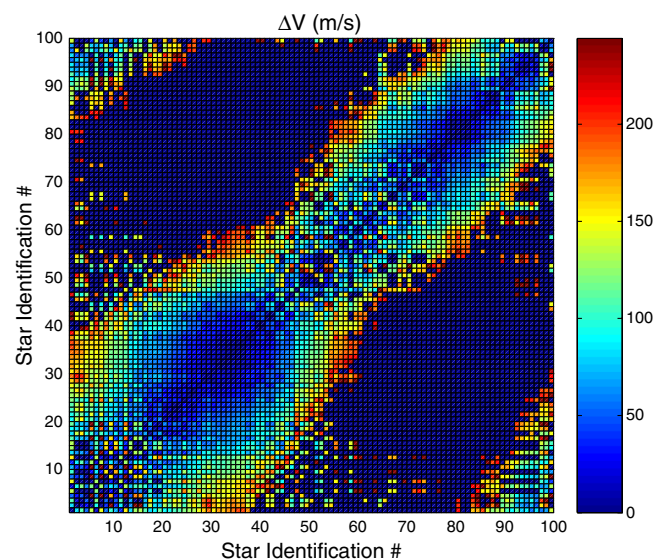


Fig. 11 Delta-V to realign between top 100 TPF-C targets with SMART-1 capabilities ($R = 50,000$ km and $\Delta t = 2$ weeks).

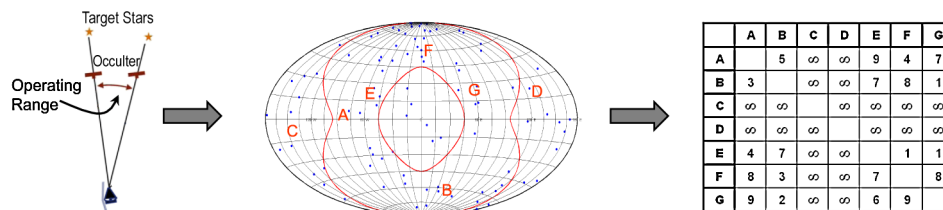


Fig. 12 Operating range of the occulter (left). Operation constraints shown on a sky map (center). Resultant TDTSP matrix (right).

mission scenarios. In particular, the question of which of the trajectory optimization approaches lead to a mission that maximizes scientific return within reasonable constraints on thruster capability, vehicle mass, and mission constraints (such as observing directions) is investigated. This is achieved by using the costs established for each control strategy and each target star to form a simple graph. The graph can then be searched for optimal mission ordering of observations. The approach taken in this section is to fix the number of observations and solve the two associated TDTSPs for the set of minimum-time and minimum-fuel trajectories. If the result exceeds the mission time or the total fuel available, the number of observations are reduced and the problem is resolved; if the result is less than the total mission time or total fuel available, the number of observations is increased. This procedure is repeated until a mission scenario with the maximum number of scientific observations under realistic constraints on the spacecraft is obtained.

A. Defining the Global Optimization Problem

The goal of the optimization is to maximize the number of imaging sessions for a given amount of fuel and/or mission time. This is a difficult optimization problem to formulate and solve, so instead, a related subprogram is solved and iterated until the maximum number of observations are reached. The used subprograms search for the optimal sequencing and timing of observations that minimize the total time given the minimum-time path between each pair of stars or that minimizes the total fuel given the minimum-fuel trajectory between each pair. To this aim, a matrix is built where each entry is the cost associated with the transfer between the star in row i and the star in column j ; the cost then is the sum of each entry in the tour. This is similar to the classical TSP where the matrix of transfer costs is referred to as the TSP matrix.

The optimal imaging problem is complicated by the presence of constraints and the fact that the cost matrix is time varying. Since the telescope is moving on its halo orbit and about the sun during observations, the cost matrix changes after each observation. This is known as a TDTSP. There also exist dynamic constraints that vary across the mission depending on the mission time, location of the telescope, and the past history of observations.

The first constraint is that the trajectories have to obey Newton's second law. This is satisfied by using the trajectories found in the previous section. Second, the reflection of sunlight from the occulter to the telescope interferes with the imaging of the planetary system. This constrains the occulter to be between approximately 45 to 95 deg from the sun direction (see Fig. 12). The mission requirements also impose other constraints on the sequencing that are not shown in this figure. To ensure that the images of the planetary system of interest do not produce the same results, the minimum-time between reimagining of a target is six months.

Figure 12 graphically illustrates the TDTSP with dynamical constraints for the occulter imaging problem. Due to reflection of the sunlight, only the stars confined within the curved lines are observable at the given instance. By including this constraint, the global optimization problem is converted to the search for the best ordering of target stars, where the Delta-Vs between the targets are shown on the TDTSP matrix (the numbers in this figure are for illustrative purposes only). In the figure, inaccessible stars (in this example, these are the stars labeled as C and D) are shown as ∞ . In the next section, the mathematical description of the TSP is presented, and then, how the cost function and constraints can be fit into that formalism is explained.

B. Classical Traveling Salesman Problem

In the classical TSP, a salesman must visit a given number of cities, for which the distances from one another are known, by the shortest possible route. The salesman's optimal path, which starts and ends in the same city, must include all cities once and only once.

Mathematically, this problem can be formulated by using a graph. The nodes and the arcs of this graph correspond to the cities and the route between cities, respectively. The TSP then becomes an assignment problem on the graph, where every node has one and only one arc leading toward it and one and only one leading away from it. This can be expressed by employing the variable

$$x_{ij} = \begin{cases} 1 & \text{if arc}(i, j) \text{ is in the tour,} \\ 0 & \text{otherwise} \end{cases} \quad (58)$$

for $i = 1, 2, \dots, n$ and $j = 1, 2, \dots, n$, and where n is the number of cities, or in the telescoping mission case, stars to visit.

On this graph, the TSP becomes the arc length minimization problem given below:

$$\begin{aligned} \min \sum_{i,j} c_{ij} x_{ij} \quad \text{s.t.} \quad \sum_i x_{ij} = 1 \quad \forall j \neq i \\ \sum_j x_{ij} = 1 \quad \forall i \neq j \quad x_{ij} \in \{0, 1\} \quad \forall i, j \end{aligned} \quad (59)$$

Here, c_{ij} are the elements of the cost matrix c . Every element of this matrix represents the distance between two cities.

However, this formulation may not give the desired, single loop that connects all the nodes. Multiple, unconnected loops, or subtours, may result. To overcome this problem, additional constraints must be added to the formulation. The Miller-Tucker-Zemlin formulation [25], which introduces new variables u_i for $i = 1, \dots, n$ for subtour exclusion, is one of the most well-known formulations:

$$\begin{aligned} u_1 = 1 \quad 2 \leq u_i \leq n \quad \forall i \neq 1 \\ u_i - u_j + 1 \leq (n-1)(1 - x_{ij}) \quad \forall i \neq 1, \quad \forall j \neq 1 \end{aligned} \quad (60)$$

The constraint formulation given in Eq. (60) is satisfied when the position of node i in the tour is u_i .

While there exist exact solution methods for the TSP, such as dynamic programming, the cutting-plane method, and branch-and-bound methods, the computation time is proportional to the exponent of the number of cities. For those who are interested in exact solutions of the TSP, CONCORDE is the current state-of-the-art software.[†]

When the exact optimal solution is not necessary, heuristic methods can be used, which quickly construct good, feasible solutions with high probability. These methods can find solutions for large problems consisting of millions of cities in a moderate time span while only deviating 2–3% from the optimal solution (see Gutin and Punnen [26] for detailed experimental analysis of the heuristic methods).

Since this study focuses on the analysis of the mission concept, exact solutions are not necessary at this stage. In Fig. 13, a suboptimal solution for the TSP problem for the top 100 TPF-C targets is given. The solution was obtained using the simulated annealing method. The numerical implementation of this heuristics is discussed in Sec. III.C.

[†]Data available at <http://www.tsp.gatech.edu/concorde.html> [retrieved 5 January 2007].

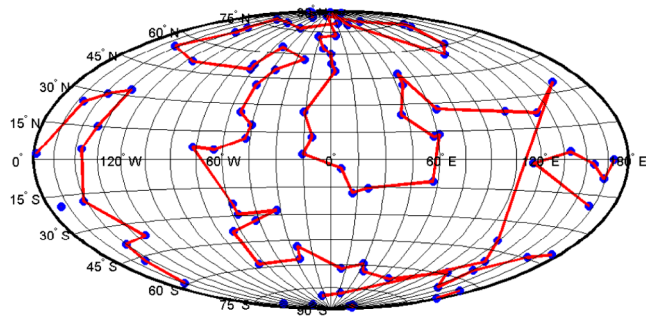


Fig. 13 Traveling salesman solution to the top 100 TPF-C targets shown on a sky map.

C. Numerical Methods Employed for Solving the Global Optimization Problem

As discussed, the exact solution methods for the optimization problem were not used. Instead, heuristic methods, which deviate only a few percent from the optimal solution and quickly construct good, feasible solutions with high probability, are employed. While solving the classical TSP, the tabu search [27], ant colony optimization [28], cross-entropy [29], genetic algorithm [30], and simulated annealing methods [31] were implemented. All performed well and converged to the correct results for the test cases.

The genetic algorithm method was ruled out as a viable candidate due to being too slow to be useful in our study. The ant colony optimization and cross-entropy methods employ a swarm of candidate solutions. These methods are not suitable for the problem at hand because of the existence of a large number of constraints. As far as the cross-entropy method is concerned, one infeasible solution in a group would bring the statistical average of the group up, but trying to impose the constraints on the elements is against the spirit of the swarms of trials and averaging. As for the ant colony optimization, it is not apparent how the constraint can be imposed that prevents the same star from being revisited before a certain amount of time.

For the fuel-optimal case, a simulated annealing method was used rather than the tabu search method since, due to the constraints, the optimal solution and initial feed might be in separated parts of the search space, and random motion given in simulated annealing might be of use to get out of local minima.

In the time-optimal case, the fact that the cost function cannot be obtained beforehand complicates the employment of the annealing method. More important, the constraints are no longer known beforehand and instead change with each neighbor operator. As a result, a branching algorithm was used where the constraints were dealt with as they arose.

1. Simulated Annealing for the Fuel-Optimal Case

In Appendix B, the algorithm that was used for the simulated annealing is explained. For this algorithm, a neighbor function has to be defined that is an operator that converts one tour into another by using exchanges or moves of the sequence vector. This function defines an associated neighborhood for each tour that can be obtained with a single function operation. Incremental improvements in the cost function are obtained by continually moving from one neighbor to a better one, with a lower cost. This is done by repeated use of the neighbor function. Finally, the optimal solution is obtained when there are no better neighbors left.

The 2-opt operation is the most famous and most tested of the simple neighbor operator functions. The 2-opt operator removes two edges and replaces these with two different edges that reconnect the fragments in the reverse order. The 2-opt was the first method of choice, but it failed to give good results. Because of the high number of constraints involved in the problem, a constraint was broken almost every time when a part of the sequence was reversed.

Consider that, as the simulated annealing proceeds, the energy of the state will be lower than that of a random state. Thus, if the neighbor function results in arbitrary states, these moves will all be

rejected after a few steps. Therefore, in simulated annealing, the neighbor function should be chosen such that the neighbors and the current tour have similar energy levels. Thus, as the neighbor function, swapping of the two consecutive rather than arbitrary stars was chosen. The notation $\text{swap}(i, j)$ is used for the operation of changing the places of the i th and j th elements of the X vector that contains the visiting sequence.

Additionally, if the operator does not obey the constraints by default, many fruitless trials result. This was avoided by choosing the initial guess to satisfy all the constraints and by making sure that all the neighbor permutations satisfy the constraint. When swapping the stars in consecutive positions, whether the swap operation leads to a minimum distance between the pair partners, a star and its revisit partner, of less than N_{revisit} , was checked [see Eq. (A6)]. If so, the swap is not performed and another random element i is chosen to swap i th and $(i + 1)$ th elements. This ensures that, as long as the initial sequence obeys the minimum separation between pairs of less than N_{revisit} , the neighbor will also obey this constraint. By not breaking any constraints, the algorithm is able to move through the neighborhood quickly.

However, the neighbor function should be able to reach every possible state of the system, and the swapping that is described above may not ensure this property because it is done in pairs. To overcome this problem, three more operators that enlarge the neighborhood sufficiently were used to avoid getting stuck in local minima. These are the following operators:

1) Swap position of two random stars and their revisit partners: $\text{swap}(u_i, u_j)$ and $\text{swap}(u_{i+n}, u_{j+n})$.

2) Mutate visit locations of random stars: $\text{swap}(u_i, u_j)$. If the resultant sequence gives rise to a minimum distance between the pairs that is less than N_{revisit} , the swap is not performed and another random pair is chosen.

3) Mutate visit locations of random star revisit partners: $\text{swap}(u_{i+n}, u_{j+n})$. If the resultant sequence gives rise to a minimum distance between the pairs that is less than N_{revisit} , the swap is not performed and another random pair is chosen.

These operators were used less frequently than the consecutive pair swaps for a total of 10% of the time for each operator as opposed to 70% for the swapping of the consecutive pairs in order to allow a fast and efficient local search.

2. Branching for Time-Optimal Case

In the branching algorithm, all the possible moves from a given initial star location are considered. Each move is the first element of a possible visiting sequence. From all these sequences, all the possible second elements are considered, and the algorithm proceeds in this manner. This leads to an exponential amount of possible sequences to be tried and stored, which is not practical. Thus, after every stage, an elimination of some of the sequences is necessary. There are many possible approaches to this selection. While the most obvious approach is to eliminate the sequences with the highest cost. The downside of this approach would be that these eliminated high-cost sequences may in the later stages lead to better results; thus, a diversification, as in the simulated annealing case, may be useful. Different diversification methods were experimented with, but these methods did not lead to better results. Thus, only the criterion of cost was used.

When, in the end, the sequence length reaches the total imaging sessions, the list element with the lowest cost is taken as the optimal solution. Unfortunately, this algorithm will lead to local minima, but the solution of the full problem is prohibitively difficult to obtain. The advantage of this algorithm is that the constraints of sun avoidance, minimum revisit time, and no revisit after two visits are satisfied in the final solution with minimal computational effort.

D. Results: Performance of SMART-1 as an Occulter

A feasibility study is performed where the mission is constrained to use the SMART-1 spacecraft with all its limitations, including the fuel onboard and maximum thrust. In Sec. II.D, all the necessary minimum-fuel and minimum-time trajectories for the SMART-1

spacecraft as an occulter are computed and the TSP matrices at any given time are obtained. Now, the global optimization is examined using these results.

It is assumed that the spacecraft continues imaging until the fuel is depleted, which is calculated via Eq. (46). The fuel consumption is found for an initial guess of N_{\max} , and this value is increased until the fuel consumption is more than the fuel onboard, which gives the maximum possible observations. Figure 14 shows the results that would be obtained if a minimum-fuel strategy were employed. Here, the maximum two revisits per star constraint were taken out because hundreds of observations with this constraint mean that the occulter ends up revisiting the other stars repeatedly. Since the fuel onboard is limited, a more spendthrift fast slew approach, where the time between the imaging sessions is decreased, leads to a decrease in the total number of observations. The last data points at 20,000 km for one week and 70,000 km for two weeks are very restrictive, since they give very few options for consecutive targets. As a result, they do not provide the flexibility that is needed in a real-life mission.

Figure 15 shows the results that would be obtained if a minimum-time transfer strategy, which uses continuous full thrust, were employed (see Table 1 mission). This figure shows that, as the radius of the formation increases, the total number of imaging sessions decreases. When this is compared with Fig. 14, it is apparent that the minimum-time strategy trades off the speed of observations against the total number of observations.

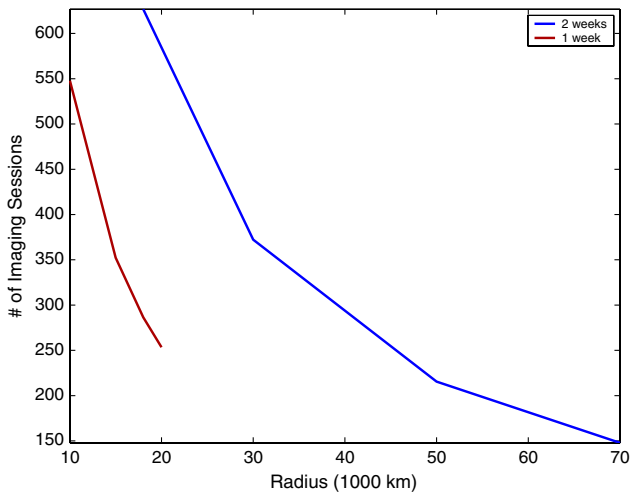


Fig. 14 Total number of imaging sessions versus the radius for the fuel-optimal control case (with SMART-1 capabilities).

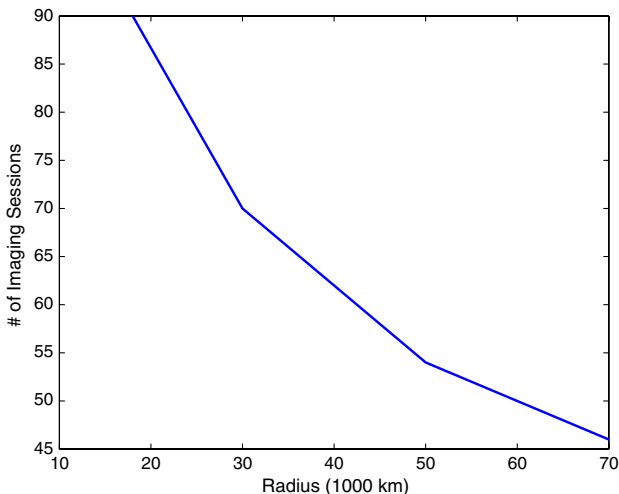


Fig. 15 Total number of imaging sessions versus the radius for the time-optimal control case (with SMART-1 capabilities).

Even though the results from Figs. 14 and 15 should be treated as the optimistic upper bounds for the number of possible imaging sessions, it is apparent that, notwithstanding the difficulties, the mission is within reach of the current technology. The Delta-V requirements for the occulter are reasonable. With the next generation of thrusters, it should be possible to maneuver the approximately 40-m-diam occulter to do sufficient imaging to be able to find Earth-like planets.

IV. Conclusions

In this paper, the optimal configuration of a satellite formation consisting of a telescope and an occulter around sun–Earth L2 halo orbits used for imaging extrasolar planets is studied. Trajectory optimization of the occulter motion between imaging sessions of different stars is performed, and the global optimization problem is solved for missions consisting of a telescope and a single occulter employing heuristic methods. Performance of an example spacecraft, SMART-1, as an occulter is analyzed. This study introduced a baseline optimal mission design for the occulter-based imaging mission and enables a tradeoff study comparing different occulter-based approaches with one another as well as with their alternatives.

There are still many issues to overcome before a mission of this sort can be feasible, such as designing an alignment system for the telescope–occulter formation and designing an optical system that can perform robustly under various deformations of the occulter due to thermal and mechanical forces. The results show that, using available technology and the optimal trajectories obtained in this study, necessary thrust specifications and fuel consumption for formation control are within the current spacecraft mission capabilities. Thus, it is feasible to design an occulter-based telescope mission around L2 from an orbital design perspective.

Appendix A: Mathematical Formulation of the Global Optimization Problem

In this appendix, the mathematical formulation for the realignment problem is obtained, starting from the classical TSP formulation. There are four major differences between the classical TSP and the realignment problem. First, the cost matrix in this case is time-dependent due to the motion of the telescope on the halo orbit, the change in the star directions relative to the telescope, and the evolution of the exclusion zone. Second, additional constraints must be satisfied. Third, the occulter may visit some of the star targets more than once. And finally, the occulter does not have to visit all the possible star targets.

The traveling occulter problem is formulated given the following parameters: the total number of observations N_{tot} , the identification number of the stars that can be imaged more than once i_r , and the slew time between imaging sessions Δt . For the sake of simplicity, it is assumed that the maximum number of visits to any given star is two. The results can easily be extended to the case with more than two visits. The formulation of the problem is set such that the multiple occulter case is obtained with minimal modification of this formulation.

I. Cost Function

First, the cost function for the problem is defined with only a single measurement for each star. The time interval between each observation Δt is assumed to be constant in order to simplify the problem. Then, t_i , the time when the i th target is being imaged, becomes $\Delta t u_i$, which is only a function of how many observations were conducted before the current target. Thus, the cost matrix that is to be minimized can be expressed as

$$\min \sum_{i,j} c(i, j, u_i) x_{ij} \quad (\text{A1})$$

In this formulation, $c(i, j, u_i)$ is a three-dimensional matrix at each time instance given with u_i , which can be precomputed.

Elements of $c(i, j, u_i)$ are the final cost of the optimal trajectories found in the last section. At each time interval, the constraints, such as the stars that are nonimageable due to their location relative to the sun, are calculated. For the stars that cannot be observed at that time, the $c(i, j, u_i)$ is set to infinity.

The sequence after the maximum visit number should not matter in the total cost computation. To ensure that it is excluded, the matrix elements of $c(i, j, u_i)$ for all u_i greater than the user-specified maximum number of total observations N_{tot} are set to zero:

$$c(i, j, u_i) = 0 \quad \text{for } u_i \geq N_{\text{tot}} + 1 \quad (\text{A2})$$

Thus, the algorithm only minimizes cost for the Delta-V budget up to this value and does not take into account the remaining nodes.

II. Including the Revisits into the Formulation

In this section, a method to include the option of revisiting sample stars with identification numbers i_r is introduced into the formulation. As stated, it is assumed that the maximum number of imaging of a given star is two. Higher numbers can easily be introduced into the formulation without loss of generality.

First, the number of nodes are doubled such that each star now corresponds to two nodes: one for the first visit and the other for the second visit. The indices i and j are redefined to be double the size to $i = 1, 2, \dots, 2n$ and $j = 1, 2, \dots, 2n$, where n is the number stars. In this notation, elements of i and j from 1 through n represent a first visit of a target star with the identification number i or j . The elements from $n + 1$ through $2n$ represent a second visit of a target star with the identification number $i - n$ or $j - n$. Correspondingly, the cost matrix is redefined to be double the size:

$$c(i, j, u_i) := \begin{pmatrix} c(i, j, u_i) & c(i, j, u_i) \\ c(i, j, u_i) & c(i, j, u_i) \end{pmatrix} \quad (\text{A3})$$

If a star with identification number k is not allowed to be revisited, the cost for a second visit is set to infinity (or a very large number):

$$c(k + n, :, :) = \infty, \quad c(:, k + n, :) = \infty \quad (\text{A4})$$

This formulation enables keeping the TSP formulation for the x_{ij} :

$$\begin{aligned} \sum_i x_{ij} &= 1 \quad \forall j \neq i & \sum_j x_{ij} &= 1 \quad \forall i \neq j \\ x_{ij} &\in \{0, 1\} \quad \forall i, j \end{aligned} \quad (\text{A5})$$

The revisits, if they happen, should be after a certain amount of time. For a given star with identification number i and position in the sequence u_i , its revisit partner with position u_{i+n} should be separated by a minimum distance:

$$u_i + N_{\text{revisit}} \leq u_{i+n} \quad (\text{A6})$$

where n is the number of stars of interest, and N_{revisit} is the minimum reimagining interval. These constraints ensure that the revisit only happens after a certain amount of time has passed. Since the time between each observation is assumed to be constant, $t_i = \Delta t u_i$ is only a function of how many observations were conducted before. For example, for a realignment maneuver of two weeks, and a minimum allowable revisit time of six months, $N_{\text{revisit}} = 12$.

III. Full Formulation

The full formulation for the mathematical model can thus be written as

$$\begin{aligned} \min \quad & \sum_{i,j} c(i, j, u_i) x_{ij} \quad \text{s.t.} \quad \sum_i x_{ij} = 1 \quad \forall j \neq i \\ & \sum_j x_{ij} = 1 \quad \forall i \neq j \quad u_1 = 1 \quad 2 \leq u_i \leq 2n \quad \forall i \neq 1 \\ & u_i - u_j + 1 \leq (2n - 1)(1 - x_{ij}) \quad \forall i \neq 1, \quad \forall j \neq 1 \\ & u_i + N_{\text{revisit}} \leq u_{i+n} \quad \forall i \quad x_{ij} \in \{0, 1\} \quad \forall i, j \end{aligned} \quad (\text{A7})$$

where c is a precalculated three-dimensional matrix. For the minimum-fuel problem, the elements of c are the Delta-V's calculated in the previous sections. Without loss of generality, u_1 is set to one, which can be changed for different starting stars.

For the minimum-time optimization problem, the elements of the c matrix are the time to go between each target. In this case, the time spent between each realignment is no longer a constant. The cost and the constraints that are associated with the arc $i - j$ are now dependent on time t_i at position u_j .

The time at a given arc can be expressed as the sum of all the costs, or the time to go, before that node:

$$\begin{aligned} t_1 &= 0 \\ t_k &= \sum_{i,j} c(i, j, t_i) x_{ij} \quad \forall i \quad \text{such that } u_i = 1, \dots, k-1 \quad \text{and} \\ & \quad \forall j \quad \text{such that } u_j = 2, \dots, k \end{aligned} \quad (\text{A8})$$

Here, the indices of the stars that have already been visited must first be identified from the elements of u . Then, the total time is calculated by summing all the previous time intervals. The cost function c is a continuous function of time, since the observable stars change with time while the time is dependent upon all the previous observations. This formulation is a much more complicated nonlinear programming problem.

Appendix B: Simulated Annealing

Developed by Kirkpatrick et al. [31], simulated annealing is a global optimization method suitable for problems with a large search space. The method is inspired by the way crystalline structures are formed in the thermal annealing process, such as the production of high-strength steel. The analogy between the physical annealing process and the numerical optimization is such that the temperature change is akin to the time spent in the optimization, and the energy level is analogous to the cost function to be minimized. Similar to the physics of atoms under the annealing process, simulated annealing generates random solutions in the neighborhood of the old one. Initially, when the temperature is high (the initial stages of optimization), random moves that lead to higher energy (higher cost) levels are allowed frequently, but as the system cools down (optimization time increases), the tendency to allow moves that increase the energy is reduced. The algorithm becomes more like a downhill search method.

Algorithm B1 is the pseudocode for the simulated annealing algorithm used in the global optimization problem.

In the algorithm, X is a vector that contains the visiting sequence of each star (and visiting partners if they exist). Temperature is represented by T , the freezing temperature is represented by T_{min} , and the cooling constant is represented by κ . Three functions are used in the algorithm; $\text{random}()$ is a uniform-distribution random number generator in the interval $(0, 1)$, cost is the cost function for a given visiting sequence, and neighbor is a function that generates random visiting strings in the neighborhood of X .

Algorithm B1 Simulated annealing

```

Input:  $X_0, T_{\text{min}}, \kappa$ 
energy = cost( $X_0$ )
 $X = X_0$ 
while  $T > T_{\text{min}}$  do
   $X_{\text{new}} = \text{neighbor}(X)$ 
  energynew = cost( $X$ )
   $\delta = \text{energy} - \text{energy}_{\text{new}}$ 
  if  $\delta > 0$  or  $\exp(\delta/T) > \text{random}()$ , then
     $X = X_{\text{new}}$ 
    energy = energynew
     $T = T * \kappa$ 
  end if
end while
Output:  $X$ , energy

```

For the constants in the algorithm, a cooling constant of ~ 0.99 and initial temperatures in the range of $10\text{--}40^\circ$ gave good results. The freezing temperature is set to be 1° .

As for the functions, the cost function defined in the previous sections are used. This cost function can be rewritten in terms of X , the visiting sequence vector, as

$$\min \sum_k c(X(k), X(k+1), k) \quad (\text{B1})$$

References

- [1] Beckwith, S. V. W., "Detecting Life-Bearing Extrasolar Planets with Space Telescopes," *Astrophysical Journal*, Vol. 684, Sept. 2008, pp. 1404–1415.
doi:10.1086/590466
- [2] Spitzer, L., "The Beginnings and Future of Space Astronomy," *American Scientist*, Vol. 50, 1962, pp. 473–484.
- [3] Marchal, C., "Concept of a Space Telescope Able to See the Planets and Even the Satellites Around the Nearest Stars," *Acta Astronautica*, Vol. 12, 1985, pp. 195–201.
doi:10.1016/0094-5765(85)90061-X
- [4] Copi, C. J., and Starkman, G. D., "The Big Occulting Steerable Satellite (BOSS)," *Astrophysical Journal*, Vol. 532, 2000, pp. 581–592.
doi:10.1086/308525
- [5] Schultz, A. B., Jordan, I. J. E., Kochte, M., Fraquelli, D., Bruhweiler, F., Hollis, J., Carpenter, K., Lyon, R., DiSanti, M., Miskey, C., Leitner, J., Burns, R., Starin, S., Rodrigue, M., Fadali, M. S., Skelton, D., Hart, H. M., Hamilton, F., and Cheng, K.-P., "UMBRAS: A Matched Occulter and Telescope for Imaging Extrasolar Planets," *Proceedings of SPIE High-Contrast Imaging for Exo-Planet Detection*, Vol. 4860, SPIE, Bellingham, WA, 2003, pp. 54–61.
- [6] Simmons, W. L., "A Pinspeck Camera for Exo-Planet Spectroscopy," M.S. Thesis, Dept. of Mechanical and Aerospace Engineering, Princeton Univ., Princeton, NJ, 2005.
- [7] Cash, W., Schindhelm, E., Arenberg, J., Polidan, R., Kilston, S., and Noecker, C., "The New Worlds Observer: Using Occulters to Directly Observe Planets," *Society of Photo-Optical Instrumentation Engineers (SPIE) Conference Series*, Vol. 6265, SPIE, Bellingham, WA, July 2006, Paper 62651V.
- [8] Kasdin, N. J., Cady, E. J., Dumont, P. J., Lisman, P. D., Shaklan, S. B., Soummer, R., Spergel, D. N., and Vanderbei, R. J., "Occulter Design for THEIA," *Society of Photo-Optical Instrumentation Engineers (SPIE) Conference Series*, Vol. 7440, SPIE, Bellingham, WA, Aug. 2009, pp. 744005–8.
- [9] Vanderbei, R. J., Cady, E., and Kasdin, N. J., "Optimal Occulter Design for Finding Extrasolar Planets," *Astrophysical Journal*, Vol. 665, 2007, pp. 794–798.
doi:10.1086/519452
- [10] Kolemen, E., Kasdin, N. J., and Gurfil, P., "Multiple Poincaré Sections Method for Finding the Quasiperiodic Orbits of the Restricted Three Body Problem," *Celestial Mechanics and Dynamical Astronomy* (to be published).
- [11] Cash, W., Green, J., Kasdin, N. J., Spergel, D., Campbell, D., Kuchner, M., Peterson, L., Oegerle, W., Polidan, R., Lindler, D., Noecker, M., Arenberg, J., Gendreau, K., Heap, S., Stern, A., Kilston, S., Kienlen, M., Seager, S., and Vanderbei, R., "New Worlds: A Mission of Discovery," NASA TR 06-DISC06-0006, 2006.
- [12] Brown, R. A., "Single-Visit Photometric and Observational Completeness," *Astrophysical Journal*, Vol. 624, 2005, pp. 1010–1024.
doi:10.1086/429124
- [13] Perryman, M. A. C., Lindegren, L., Kovalevsky, J., Hoeg, E., Bastian, U., Bernacca, P. L., Crézé, M., Donati, F., Grenon, M., van Leeuwen, F., van der Marel, H., Mignard, F., Murray, C. A., Le Poole, R. S., Schrijver, H., Turon, C., Arenou, F., Froeschlé, M., and Petersen, C. S., "The Hipparcos Catalogue," *Astronomy and Astrophysics*, Vol. 323, July 1997, pp. L49–L52.
- [14] Kaplan, G. H., Hughes, J. A., Seidelmann, P. K., Smith, C. A., and Yallop, B. D., "Mean and Apparent Place Computations in the New IAU System. 3: Apparent, Topocentric, and Astrometric Places of Planets and Stars," *Astronomical Journal*, Vol. 97, April 1989, pp. 1197–1210.
doi:10.1086/115063
- [15] Standish, E. M., "JPL Planetary and Lunar Ephemerides, DE405/LE405," Jet Propulsion Lab., Interoffice Memo. 312-F-98-048, 1998, <http://iau-comm4.jpl.nasa.gov/de405iom/de405iom.pdf> [retrieved 2011].
- [16] Gómez, G., Masdemont, J., and Simó, C., "Quasihalo Orbits Associated with Libration Points," *Journal of the Astronautical Sciences*, Vol. 46, No. 2, 1999, pp. 1–42.
- [17] Dormand, J. R., and Prince, P. J., "High Order Embedded Runge–Kutta Formulae," *Journal of Computational and Applied Mathematics*, Vol. 7, No. 1, 1981, pp. 67–75.
doi:10.1016/0771-050X(81)90010-3
- [18] Bryson, A. E., and Ho, Y. C., *Applied Optimal Control*, Hemisphere, New York, 1975, Chap. 2, pp. 42–67.
- [19] Gill, P. E., Murray, W., and Saunders, M. A., "SNOPT: An SQP Algorithm for Large-Scale Constrained Optimization," *SIAM Journal on Optimization*, Vol. 12, No. 4, 2002, pp. 979–1006.
doi:10.1137/S1052623499350013
- [20] Wächter, A., and Biegler, L. T., "Line Search Filter Methods for Nonlinear Programming: Motivation and Global Convergence," *SIAM Journal on Optimization*, Vol. 16, No. 1, 2005, pp. 1–31.
doi:10.1137/S1052623403426556
- [21] Kierzenka, J., and Shampine, L. F., "A BVP Solver Based on Residual Control and the Matlab PSE," *ACM Transactions on Mathematical Software*, Vol. 27, No. 3, 2001, pp. 299–316.
doi:10.1145/502800.502801
- [22] Kirk, D. E., *Optimal Control Theory: An Introduction*, Prentice–Hall, Englewood Cliffs, NJ, 1970, Chap. 5, pp. 184–328.
- [23] Stengel, R. F., *Optimal Control and Estimation*, Dover, New York, 1994, Chap. 3, pp. 184–273.
- [24] MacKenzie, R., Lazaro Salvador, D., and Milligan, D., "Orbit Determination for the SMART-1 mission," *18th International Symposium on Space Flight Dynamics*, Vol. 548, ESA, France, 2004, p. 181.
- [25] Miller, C. E., Tucker, A. W., and Zemlin, R. A., "Integer Programming Formulation of Traveling Salesman Problems," *Journal of the Association for Computing Machinery*, Vol. 7, No. 4, Oct. 1960, pp. 326–329.
doi:10.1145/321043.321046
- [26] Gutin, G., and Punnen, A. P. (eds.), *Travelling Salesman Problem and Its Variations*, Vol. 12, Combinatorial Optimization, Kluwer Academic, New York, 2002, Chap. 9, pp. 369–445.
- [27] Glover, F., "Tabu Search: Part 1," *ORSA Journal on Computing*, Vol. 1, No. 3, 1989, pp. 190–206.
doi:10.1287/ijoc.1.3.190
- [28] Dorigo, M., and Gambardella, L. M., "Ant Colony System: A Cooperative Learning Approach to the Traveling Salesman Problem," *IEEE Transactions on Evolutionary Computation*, Vol. 1, 1997, pp. 53–66.
doi:10.1109/4235.585892
- [29] De Boer, P.-T., Kroese, D. P., Mannor, S., and Rubinstein, R. Y., "A Tutorial on the Cross-Entropy Method," *Annals of Operations Research*, Vol. 134, No. 1, 2005, pp. 19–67.
doi:10.1007/s10479-005-5724-z
- [30] Holland, J. H., *Adaptation in Natural and Artificial Systems: An Introductory Analysis with Applications to Biology, Control and Artificial Intelligence*, University of Michigan Press, Ann Arbor, MI, 1975, pp. 89–120.
- [31] Kirkpatrick, S., Gelatt, C. D., and Vecchi, M. P., "Optimization by Simulated Annealing," *Science*, Vol. 220, No. 4598, May 1983, pp. 671–680.
doi:10.1126/science.220.4598.671